ISTITUTO NAZIONALE DI RICERCA METROLOGICA
Repository Istituzionale

Specific heat and entropy change at the first order phase transition of La(Fe-Mn-Si)13-H compounds

(Article begins on next page)

25 November 2024

Vittorio Basso, Michaela Küpferling, Carmen Curcio, Cecilia Bennati, Alexander Barzca, Matthias Katter, Milan Bratko, Edmund Lovell, Jeremy Turcaud, and Lesley F. Cohen

---

Specific heat and entropy change at the first order phase transition of La(Fe-Mn-Si)₁₃-H compounds

Vittorio Basso,[1,a)] Michaela Küpferling,[1] Carmen Curcio,[1,2] Cecilia Bennati,[1,2] Alexander Barzca,[3] Matthias Katter,[3] Milan Bratko,[4] Edmund Lovell,[4] Jeremy Turcaud,[4] and Lesley F. Cohen[4]

[1]*Istituto Nazionale di Ricerca Metrologica, Strada delle Cacce 91, 10135 Torino, Italy*
[2]*DISAT, Politecnico di Torino, Corso Duca degli Abruzzi 24, 10129 Torino, Italy*
[3]*Vacuumschmelze GmbH & Co. KG, Grüner Weg 37, 63450 Hanau, Germany*
[4]*The Blackett Laboratory, Imperial College, London SW7 2BZ, United Kingdom*

In this paper, we present the results of an experimental investigation on the magnetocaloric properties of hydrogenated La(Fe-Mn-Si)₁₃-H with Mn substituting Fe to finely tune the transition temperature. We measured the specific heat under magnetic field $c_p(H, T)$ and the magnetic field induced isothermal entropy change $\Delta s(H, T)$ of a series of compounds by direct Peltier calorimetry. Results show that increasing Mn from 0.06 to 0.46 reduces the transition temperature from 339 K to 270 K whilst the total entropy change due to a 1.5 T field is depressed from 18.7 J kg⁻¹K⁻¹ to 10.2 J kg⁻¹K⁻¹ and the thermal hysteresis similarly is reduced from 1.5 K to zero. In the paper, we interpret the results in terms of a magnetic phase transition changing from the first to the second order with increasing Mn content, and we discuss the value of the results for magnetic cooling applications. © 2015 AIP Publishing LLC. [http://dx.doi.org/10.1063/1.4928086]

I. INTRODUCTION

The development of magnetic refrigeration around room temperature is based on the possibility to establish material classes with a tunable Curie temperature that can be efficiently employed in different cross sections of an active magnetic regenerator.[1] Two classes of magnetic materials, both displaying first order magnetic phase transitions between ferromagnetic (FM) and paramagnetic (PM) phases with an enhanced magnetocaloric effect (MCE), are currently the most promising candidates: the La(Fe-Si)₁₃ class[2] and the MnFe(X-P) class with X = As, Ge, Si.[3,4] The transition temperature of La(Fe-Si)₁₃, which is around 200 K, can be tuned up to room temperature by partial substitution of Fe with Co,[5] but the transition is transformed into a second order type corresponding to a lower MCE. A more interesting solution is the introduction of interstitial hydrogen, which conserves the first order character and a high MCE.[2] However, the full hydrogenation, which is needed to avoid degradation aging and to have a long time stability of the material,[6] shifts the transition to about 350 K. The substitution of Fe by Mn lowers the transition temperature T_t, thereby permitting a fine tuning around room temperature.[7–9] The system with Mn is also particularly interesting because it shows a trend in which the transition passes from fully first order and hysteretic at low Mn to almost second order with no hysteresis at high Mn. It has been suggested that a transition on the border between first and second order would provide the optimal magnetocaloric properties, because it conserves a high MCE typical of a first order transition but removes the unwanted thermal hysteresis.[10] The Mn substituted La(FeSi)₁₃ represents such a system, and as such, it

deserves a detailed experimental investigation and an accurate physical comprehension.

In this paper, we have investigated fully hydrogenated LaFeₓMnᵧSi_z-H₁.₆₅ $(x+y+z=13)$ samples with variable Mn content from $y=0.06$ to 0.46. We made an experimental investigation of the MCE by direct calorimetry in magnetic field in order to determine the effectiveness of the Mn to obtain optimized MCE properties.[11–13] We find that the transition, without a magnetic field applied, passes from first order $(\Delta T_{hyst}=1.5\,K)$ at y = 0.06 $(T_t=339\,K)$ to almost second order with no hysteresis at y = 0.46 $(T_t=270\,K)$. The usable (cyclic) entropy change at $\mu_0 H=1.5$ T passes from 18.7 to 10.2 J kg⁻¹K⁻¹, while the adiabatic temperature change (as derived from the entropy versus temperature diagram) reaches its maximum of 4.4 K at the intermediate compositions. From our results, we find that a first order character of the transition combined with a small temperature hysteresis (<1 K) represents the optimal compromise for magnetic cooling applications of La(Fe-Mn-Si)₁₃-H.

II. EXPERIMENTAL

La(Fe-Mn-Si)₁₃ alloys with variable Mn content were prepared by powder metallurgy technique and hydrogenated as described in Ref. 6. Master alloys were prepared by vacuum induction melting followed by mechanical milling steps to produce fine powders. The composition of each alloy was adjusted by blending master alloys with elemental powders. Compaction of the powder blends was performed by cold isostatic pressing. The green bodies were vacuum sintered at around 1100 °C followed by an annealing treatment at 1050 °C.[5] Hydrogenation was performed on a granulate material with a particle size less than 1 mm.[9] The composition

TABLE I. Composition x, y, z of the LaFe$_x$Mn$_y$Si$_z$-H$_{1.65}$ samples under investigation with transition temperature upon heating T_h, temperature hysteresis $\Delta T_{hyst} = T_h - T_c$ and specific heat capacity c_{PM} in the paramagnetic phase, difference in entropy $s_{PM} - s_{FM}$ from FM to PM at zero field, magnetic field dependence of the transition temperature dT/dH.

x (Fe)	y (Mn)	z (Si)	T_h (K)	ΔT_{hyst} (K)	c_{PM} (J kg^{-1} K^{-1})	$s_{PM} - s_{FM}$ (J kg^{-1} K^{-1})	$\mu_0^{-1} dT/dH$ (K T^{-1})
11.22	0.46	1.32	269.7	0.0	450	12.0	4.5
11.33	0.37	1.30	285.4	0.2	450	14.5	4.8
11.41	0.30	1.29	296.6	0.4	460	16.0	4.4
11.47	0.25	1.28	303.9	0.5	460	18.0	4.0
11.55	0.22	1.23	313.7	0.7	470	18.5	4.0
11.60	0.18	1.22	320.6	0.9	480	19.0	3.9
11.66	0.14	1.20	327.5	1.2	490	20.5	3.8
11.76	0.06	1.18	339.0	1.5	500	21.5	3.6

results to be LaFe$_x$Mn$_y$Si$_z$-H$_{1.65}$ with x, y, z indicated in Table I.

Calorimetric measurements have been performed on samples made of several granules packed together (with a total typical mass around 50 mg) closed into aluminum pans. Characterization was done by commercial power compensation differential scanning calorimetry (DSC) and Peltier calorimetry under magnetic field.[11] Under zero applied field, the results of power compensation DSC and Peltier calorimetry agree within the measurement uncertainty. The Peltier setup was filled with Ar gas at ambient pressure and calibrated by sapphire sample of known heat capacity in the same condition of the sample measurement. For both power compensation and Peltier setup, we have measured the heat flux q_s as a function of temperature T_b. The temperature of the sample $T = T_b - Rq_s$ is derived from the measured temperature T_b, by taking into account the presence of a thermal contact resistance R between the sample and the calorimetric cells.[12] The thermal contact resistance R was determined by performing scans at different rates of 25, 50, and 100 mK s^{-1} at zero field and rescaling the measurements as shown in Ref. 12. The measurement uncertainty of the sample temperature is around ± 0.2 K. In Peltier calorimetry, the additional thermal resistance due to measuring cells, $R_c = 75$ KW^{-1} is taken into account as $R = R_c + R_s$, where R_s is the contact realized between the sample and the heat flux sensor. The obtained values of R_s range from 10 to 50 KW^{-1} and can be attributed to nonideal conductivity in the samples itself due the loose packing of the grains inside the sample pan. By defining $R_s = d_t/(\kappa_t A_t)$, where A_t is the sample contact area, d_t the thickness, and κ_t is the effective thermal conductivity, we find that the packing corresponds to a κ_t ranging from 0.5 to 4 WK^{-1} m^{-1}. By applying the method just described to all the measured samples we successfully obtain rate independent results, i.e., the use of the contact thermal resistance is effective to eliminate all the extrinsic kinetics. The specific heat is obtained from the measured heat flux q_s as

$$c_p = \frac{1}{m_s} \frac{q_s}{dT/dt}, \qquad (1)$$

where m_s is the sample mass. The specific entropy variation is computed from the measured heat flux q_s, by the expression

$$s - s_0 = \frac{1}{m_s} \int_0^t \frac{q_s}{T} dt, \qquad (2)$$

where the s_0 is a reference entropy value. The typical results obtained for c_p and entropy $s - s_0$ are shown in Figs. 1 and 2. Measurements have been performed upon heating and cooling to determine the temperature hysteresis. Table I reports the results of the transition temperature upon heating T_h, temperature hysteresis $\Delta T_{hyst} = T_h - T_c$ and specific heat capacity c_{PM} in the paramagnetic phase. c_{PM} is taken at a temperature well above the transition temperature where the peak is smoothed out and the specific heat becomes magnetic field independent. The transition temperatures upon heating and cooling, T_h and T_c, are derived from the measured $s(H, T)$ curves. In presence of first order transitions with hysteresis we determine T_h and T_c as the values at which the transition is at the midpoint between the PM phase and the FM phase upon heating and cooling, respectively (see Fig. 3). For each magnetic field curve, the experimental specific heat is fitted below and above the transition region, to give c_{FM} and c_{PM}, respectively. The fit to the data reveals that in the PM state, c_{PM} can be approximately taken as a constant value, while in the FM state, c_{FM} changes linearly with T as $c_{FM} = c_{FM_0} + d_{FM}(T - T_t)$ as can be seen in Fig. 4. The two entropy equations, $s_{FM}(T)$ and $s_{PM}(T)$, are both obtained by the integral $s_i = \int(c_i/T)dT + s_{0_i}$, where $i = PM$ or FM, using the fitted parameters. The difference between the integration constants $s_{0_{PM}} - s_{0_{FM}}$ is determined by the comparison with the experimental entropy curves. The transition temperature is finally obtained as the midpoint between FM and PM, i.e., the point at which the experimental curve crosses the level $(s_{PM} - s_{FM})/2$ as shown in the sketch of Fig. 3.

The magnetic field dependence of all the thermodynamic quantities was measured by Peltier calorimetry. In all cases, the magnetic field was applied along a diameter of the circle constituting the base of the thin cylindrical sample holder filled with magnetocaloric material. The heat flux q_s was measured by temperature scan experiments and the specific heat $c_p(H, T)$ and the entropy $s(H, T)$ were computed using Eqs. (1) and (2). The magnetic field induced isothermal entropy change was also measured by performing magnetic field scan experiments at selected temperatures in order to determine the reference values of the entropy change at different
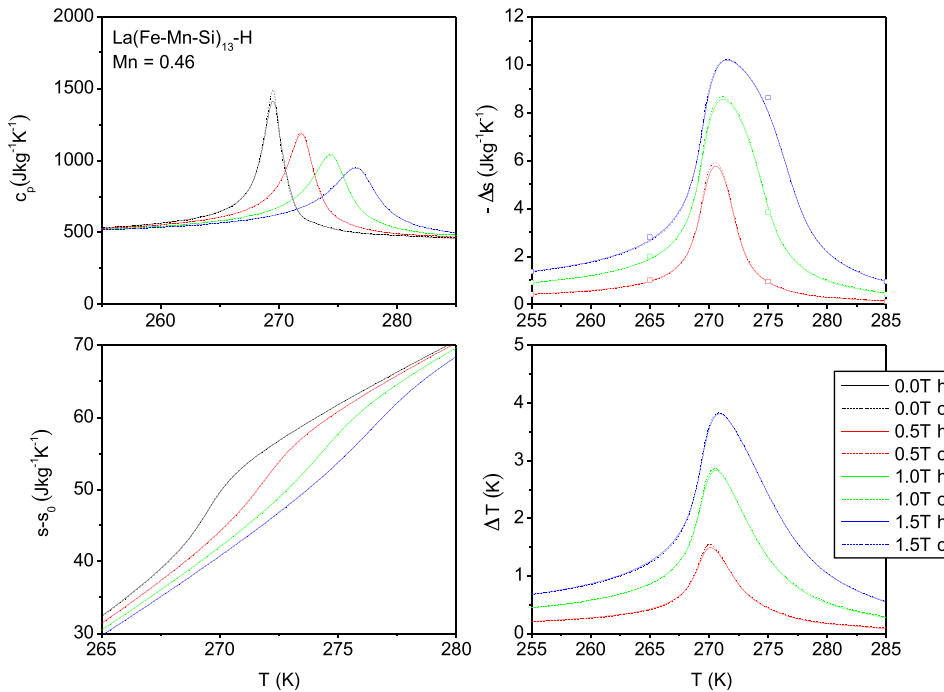
FIG. 1. Calorimetry on hydrogenated La(Fe-Mn-Si)$_{13}$ with Mn = 0.46. Top left: specific heat capacity $c_p(H, T)$; bottom left: entropy difference with respect to a low temperature reference state $s(H, T) - s_0$; top right: magnetic field induced isothermal entropy change $-\Delta s(H, T)$; bottom right: magnetic field induced adiabatic temperature change $\Delta T(H, T)$. All graphs show the results upon heating and cooling separately.

fields[11] (points in the top right panel of Figs. 1 and 2). The distance between measured points (5 K) is large enough in comparison to the hysteresis (1.5 K maximum) to avoid the minor loop effect mentioned in the literature.[17] The magnetic field induced entropy change was derived by subtracting the entropy curves at different fields $\Delta s(H, T) = s(H, T) - s(0, T)$. The plots show heating and cooling curves separately. The measurement uncertainty for the specific heat and the entropy is around $\pm 3\%$. Figs. 1 and 2 show the results of the experimental characterization obtained from calorimetry in magnetic field for two different samples. We show here, as

representative examples, the two limit cases: Mn = 0.46, the most second order, and Mn = 0.06, the most first order of the series. Figs. 1 and 2 show in the four panels: the specific heat capacity $c_p(H, T)$ (top left), the entropy difference with respect to a low temperature reference state $s(H, T) - s_0$ (bottom left), the magnetic field induced entropy change $-\Delta s(H, T)$ $= -s(H, T) + s(0, T)$ (top right), and the adiabatic temperature change $\Delta T(H, T)$ derived from the entropy plot of the bottom left panel by taking the temperature differences at the same entropy level (bottom right). All graphs show the measurements upon both heating and cooling.
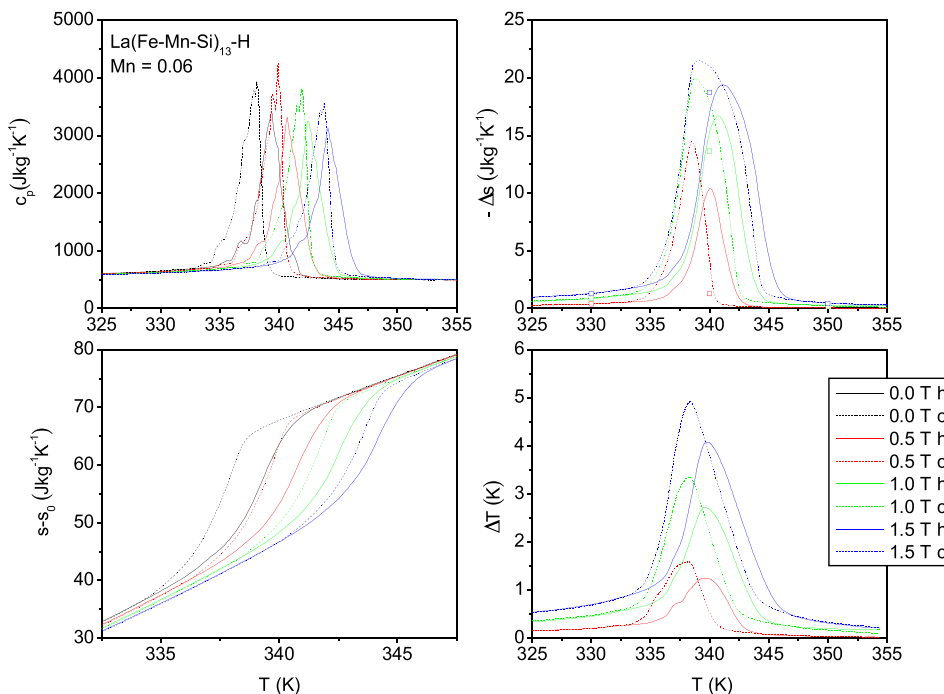

FIG. 2. Calorimetry on hydrogenated La(FeMnSi)$_{13}$ with Mn = 0.06. Same panels as in Fig. 1.
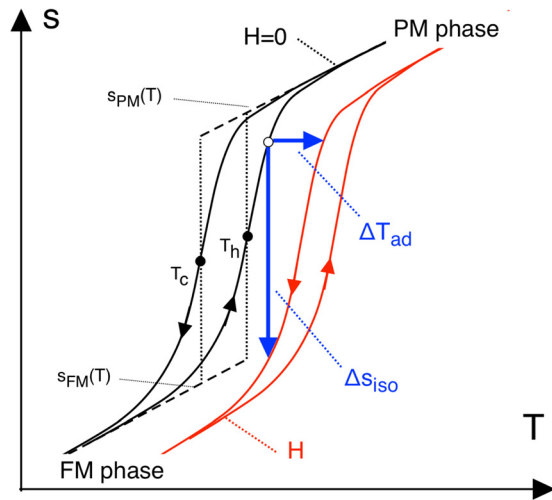
FIG. 3. Sketch of the entropy versus temperature for the case of an equation of state with hysteresis. The isothermal entropy change Δs_{iso} and the adiabatic temperature change ΔT_{ad} obtained in a cooling thermodynamic cycle are indicated. Dashed lines shows the fitting functions for the entropy in the PM and FM states $s_{PM}(T)$ and $s_{FM}(T)$. The transition temperatures T_h and T_c are defined as the midpoint of the transition between s_{FM} and s_{PM}.

III. RESULTS

The introduction of Mn is found to decrease the transition temperature from about 350 K (at Mn = 0) at a linear rate of 175 K/y_{Mn}. The same effect is present in nonhydrogenated compounds, where the Mn acts in a very similar way.[7] Mn substitution is also found to decrease the hysteresis at a rate of 4.6 K/y_{Mn}, which means that the transition kind is transformed from first to second order. Figs. 4 and 5 show the specific heat capacity for the series. Fig. 4 shows the heating and cooling at zero magnetic field. The effect of the Mn is seen in the decrease of the height of the peak of the specific heat capacity and in the disappearance of difference between heating and cooling curves. Fig. 5 shows only the heating for different magnetic fields. While at low Mn the action of the magnetic field is mainly to shift the peak c_p to the right, at high Mn it also reduces the amplitude,
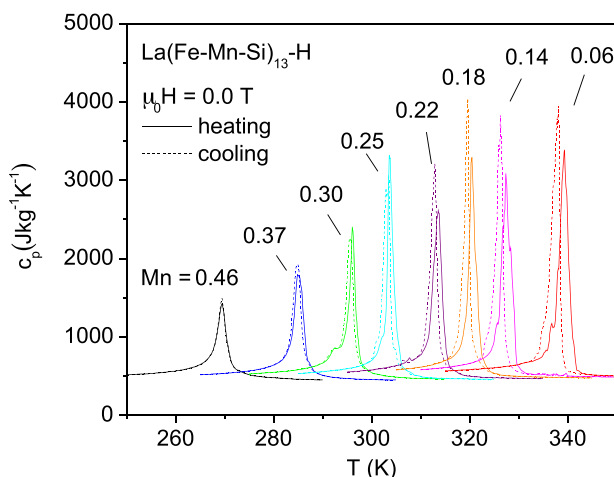

FIG. 4. Specific heat capacity of hydrogenated La(Fe-Mn-Si)$_{13}$ with different Mn content. Measurements upon heating and cooling at zero magnetic field.
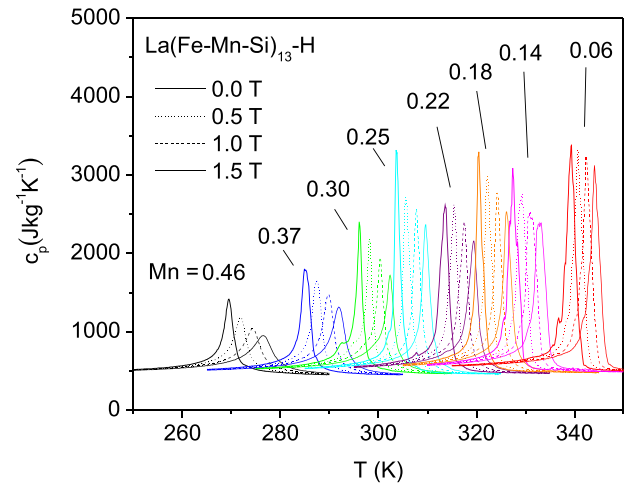

FIG. 5. Specific heat capacity of hydrogenated La(Fe-Mn-Si)$_{13}$ with different Mn content. Measurements upon heating at different magnetic fields.

suggesting that the transition is close to a second order critical point.

Information on how close the system is to the critical point can be gained by looking at the transition temperatures as a function of the magnetic field. Fig. 6 shows the magnetic phase diagram built by taking the transition temperatures upon heating and cooling. Fig. 6 also shows the lines corresponding to the linear fit of the heating and cooling points. The region enclosed between the two lines represents the metastability region in which both ferromagnetic and paramagnetic phase coexist. The critical point is at the intersection of the two lines. Fig. 6 shows how the critical magnetic field and temperature (H_{crit}, T_{crit}) are reduced as Mn content is increased until the transition is purely second order around the composition Mn = 0.46. These observations show that Mn plays a dual role: decreasing the strength of the FM coupling and decreasing the magnetoelastic coupling. The
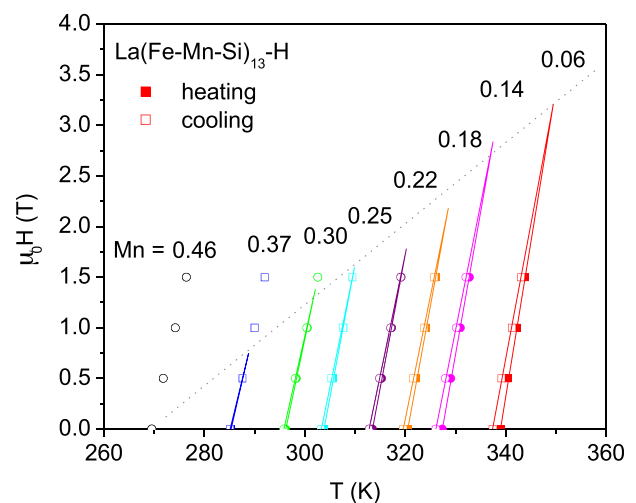
FIG. 6. Magnetic phase diagram of hydrogenated La(Fe-Mn-Si)$_{13}$ with different Mn content. Symbols are the transition temperatures upon heating T_h and cooling T_c versus magnetic field in the (H, T) diagram. Full lines are the linear fit of measured points. Heating and cooling lines intercept at the critical point (H_{crit}, T_{crit}). Dashed line is the guide for the eye of the evolution of the critical point in the (H, T) diagram with changing Mn. The dashed line crosses $H = 0$ around Mn = 0.46 indicating a second order transition.

identification of the exact position of the critical points in the phase diagram deserves a detailed experimental investigation by special methods,[14,15] which will be the subject of future investigations.

The careful characterization of hysteresis is particularly relevant for applications utilizing the magnetocaloric effect in a cyclic fashion. For a refrigerator, the cycle consists of four individual steps: (i) increasing the temperature of the active material above the temperature of the hot bath, (ii) releasing heat to the hot bath, (iii) decreasing the temperature of the active material to a temperature below the cold bath, (iv) extracting heat from the cold bath. For materials exhibiting hysteresis, the magnitude of the magnetocaloric response in each of these four steps depends on the thermal and magnetic history of the material which is generated by the four steps.[16–18] Here, we use our extensive dataset to evaluate the behavior of La(Fe-Mn-Si)-H alloys in cyclic applications. Fig. 3 shows a sketch of entropy versus temperature during heating and cooling in zero magnetic field (black lines) and some applied magnetic field (red lines) for a material exhibiting thermal hysteresis. The magnetic state of such a material can be changed either by temperature or by magnetic field. The paramagnetic state is favored by either decreasing magnetic field or by increasing temperature, while, conversely, the ferromagnetic state is stabilized by either increasing magnetic field or by decreasing temperature. Therefore, when ferromagnetism is induced by applying a magnetic field H, the thermal analogue corresponds to a cooling process, while when paramagnetism is induced by removing a magnetic field, the thermal analogue is a heating process. Even if, in principle, the calculation Δs_{iso} and ΔT_{ad} in cyclic operations should result from the details of the hysteresis branches of partial transformations in the $s - T$ diagram,[16,19] in the case of La(Fe-Mn-Si)$_{13}$-H, the situation is much simplified by the fact that the magnetic field change is always large enough to overcome the hysteresis, so that the hysteresis loop can be used as the end-point (see Fig. 3). The condition for this limit to be valid is $dT/dH \times H > T_{hyst}$ and is satisfied for all the compounds of the series also at the lower
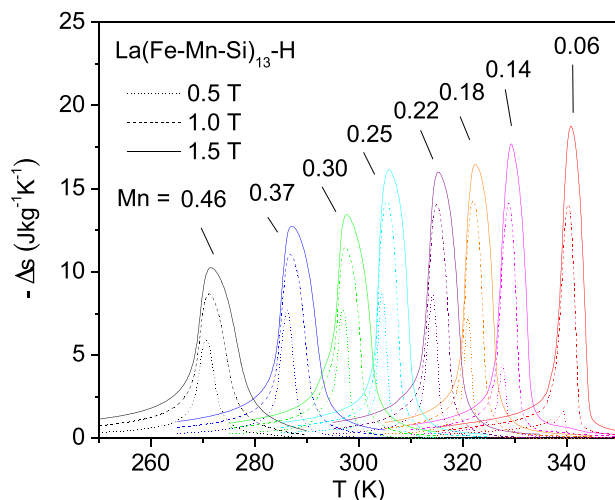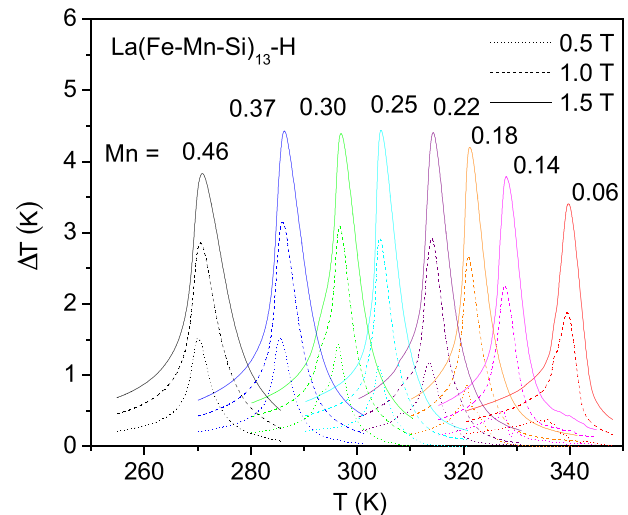

FIG. 8. Adiabatic temperature change ΔT_{ad} for cyclic processes of hydrogenated La(Fe-Mn-Si)$_{13}$ with different Mn content.

magnetic field value used (0.5 T). It follows that for the calculation of Δs_{iso} and ΔT_{ad} due to cyclic operations, the heating curve in zero magnetic field and the cooling curve in magnetic field has to be used. Hence, a cyclic operation in the hysteretic region leads to reduced Δs_{iso} and ΔT_{ad} compared to a scenario in which the previous thermal and magnetic history is deleted, as for example, by a previous reset to the PM state.[17,19] This reduction can be appreciated by looking at sample Mn = 0.06 and comparing the irreversible entropy change and temperature change obtained in Fig. 2 using heating and cooling curves separately and the reversible result of Figs. 7 and 8.

Figs. 7 and 8 show the available isothermal entropy change and adiabatic temperature change for all samples considering cyclic processes with hysteresis. Table II shows the values at the peak of Δs_{iso} and ΔT_{ad} for a field change of 1.5 T and their product $\Delta s_{iso}\Delta T_{ad}$.[20,21] In particular, the peak of the Δs_{iso} increases, while Mn is reduced, as expected for a transition which is more of the first order type. However, at the same time, at Mn less then 0.25, the peak of ΔT_{ad} becomes smaller because the hysteresis of the transition directly affects the maximum of ΔT_{ad}. When looking at the product $\Delta s_{iso}\Delta T_{ad}$ the best compromise is obtained for intermediate compositions in which the transition is sufficiently steep and first order, but the hysteresis is still small enough. In the series analyzed, it is observed that the two effects do not compensate

TABLE II. Magnetocaloric properties of hydrogenated La(Fe-Mn-Si)$_{13}$ with different Mn content at the magnetic field of 1.5 T.

Mn	T_h (K)	Δs_{iso} (J kg^{-1}K^{-1})	ΔT_{ad} (K)	$\Delta s_{iso}\Delta T_{ad}$ (J kg^{-1})
0.46	269.7	10.2	3.8	38.8
0.37	285.4	12.7	4.4	55.9
0.30	296.6	13.4	4.4	59.0
0.25	303.9	16.1	4.4	70.8
0.22	313.7	16.0	4.4	70.4
0.18	320.6	16.4	4.2	68.9
0.14	327.5	17.7	3.8	67.3
0.06	339.0	18.7	3.4	63.6

FIG. 7. Isothermal entropy change $-\Delta s_{iso}$ for cyclic processes of hydrogenated La(Fe-Mn-Si)$_{13}$ with different Mn content.

and showing that the best compromise is the one where Mn = 0.25 at which the product $\Delta s_{iso}\Delta T_{ad} = 70.8\,\mathrm{J\,kg^{-1}}$ is maximum (see Table II). Another prerequisite for building efficient solid-state heat pumps is the ability to utilize regenerative cycles such as the active magnetic regeneration (AMR) cycle.[1] In such a cycle, the transition temperature of each material has to be adjusted with regard to the neighboring materials in order to achieve the temperature spans required by the application. Here, we show a series of hydrogenated La(Fe-Mn-Si)$_{13}$ alloys covering a temperature range from 250 to 350 K with carefully adjusted transition temperatures demonstrating the potential of this material class to be employed in prototypes.

IV. CONCLUSIONS

In this paper, we have investigated the magnetocaloric properties of hydrogenated La(Fe-Mn-Si)$_{13}$ by calorimetry in magnetic field. In the set of samples with Mn increasing from 0.06 to 0.46, the transition temperature can be finely tuned from 339 K to 270 K. At the same time, the magnetic phase transition passes from first order to second order and temperature hysteresis is reduced from 1.5 K to zero. The calorimetric characterization provides the entropy as a function of temperature and magnetic field $s(H, T)$ on both heating and cooling processes from which the isothermal entropy change Δs_{iso} and the adiabatic temperature change ΔT_{ad} in cyclic (Carnot) process can be derived. By these results, we disclose the role played by temperature hysteresis on the magnetocaloric properties. In particular, we find that large values of the product $\Delta s_{iso}\Delta T_{ad}$ are reached by a compromise between sufficiently first order character of the transition with high Δs_{iso} and low hysteresis ΔT_{hyst}.

Both parameters are determined by the fact that the substitution of Fe by Mn both lowers the transition temperature T_t and shift the transition type toward second order. From our investigation it appears that the optimal cases are those in which the transition is still of the first order type. The role played by Mn is then twofold: to decrease the exchange interaction and to decrease the magnetoelastic coupling, giving rise to the first order transition. Both aspects merits further theoretical investigation to understand the origin of the physical mechanism.

ACKNOWLEDGMENTS

[1]A. Kitanovski, J. Tusek, U. Tomc, U. Plaznik, M. Ozbolt, and A. Poredos, *Magnetocaloric Energy Conversion: From Theory to Applications* (Springer, London, 2015).

[2]A. Fujita, S. Fujieda, Y. Hasegawa, and K. Fukamichi, "Itinerant-electron metamagnetic transition and large magnetocaloric effects in La(Fe$_x$Si$_{1-x}$)$_{13}$ compounds and their hydrides," Phys. Rev. B **67**, 104416 (2003).

[3]O. Tegus, E. Bruck, K. H. J. Buschow, and F. R. de Boer, "Transition-metal-based magnetic refrigerants for room-temperature applications," Nature **415**, 150 (2002).

[4]H. Yibole, F. Guillou, L. Zhang, N. H. van Dijk, and E. Bruck, "Direct measurement of the magnetocaloric effect in MnFe(P,X)(X = As, Ge, Si) materials," J. Phys. D: Appl. Phys. **47**, 075002 (2014).

[5]M. Katter, V. Zellmann, G. W. Reppel, and K. Uestuener, "Magnetocaloric properties of La(FeCoSi)$_{13}$ bulk material prepared by powder metallurgy," IEEE Trans. Magn. **44**, 3044 (2008).

[6]A. Barcza, M. Katter, V. Zellmann, S. Russek, S. Jacobs, and C. A. Zimm, "Stability and magnetocaloric properties of sintered La(Fe, Mn, Si) H Alloys," IEEE Trans. Magn. **47**, 3391 (2011).

[7]F. Wang, Y.-F. Chen, G.-J. Wang, and B.-G. Shen, "The effect of Mn substitution in LaFe$_{11.7}$Si$_{1.3}$ compound on the magnetic properties and magnetic entropy changes," J. Phys. D: Appl. Phys. **36**, 1 (2003).

[8]K. Morrison, K. G. Sandeman, L. F. Cohen, C. P. Sasso, V. Basso, A. Barcza, M. Katter, J. D. Moore, K. P. Skokov, and O. Gutfleisch, "Evaluation of the reliability of the measurement of key magnetocaloric properties: A round robin study of La(Fe,Si,Mn)-H conducted by the SSEEC consortium of European laboratories," Int. J. Refrig. **35**, 1528 (2012).

[9]M. Krautz, K. Skokov, T. Gottschall, C. S. Teixeira, A. Waske, J. Liu, L. Schultz, and O. Gutfleisch, "Systematic investigation of Mn substituted La(Fe,Si)$_{13}$ alloys and their hydrides for room-temperature magnetocaloric application," J. Alloys Compd. **598**, 27 (2014).

[10]R. P. Santana, N. A. de Oliveira, and P. J. von Ranke, "Magnetocaloric properties of compounds with first order phase transition: Hysteresis effect," J. Alloys Compd. **509**, 6346 (2011).

[11]V. Basso, C. P. Sasso, and M. Kuepferling, "A Peltier cells differential calorimeter with kinetic corrections for the measurement of c$_p$(H,T) and Δs(H,T) of magneto-caloric materials," Rev. Sci. Instrum. **81**, 113904 (2010).

[12]V. Basso, C. P. Sasso, and M. Kuepferling, "Entropy change at magnetic phase transitions of the first and second order," Int. J. Refrig. **37**, 257 (2014).

[13]V. Basso, M. Kuepferling, C. Curcio, A. Barzca, and M. Katter, "Thermal hysteresis in La(Fe,Mn,Si)$_{13}$-H alloys," in *Proceedings of the 6th IIF-IIR International Conference on Magnetic Refrigeration: Refrigeration Science and technology IIR-IIF, 2014-4, Victoria, BC, Canada, 7–10 September 2014*, ISBN: 9782362150074.

[14]K. Morrison, M. Bratko, J. Turcaud, A. Berenov, A. D. Caplin, and L. F. Cohen, "A calorimetric method to detect a weak or distributed latent heat contribution at first order magnetic transitions," Rev. Sci. Instrum. **83**, 033901 (2012).

[15]K. Morrison, A. Dupas, Y. Mudryk, V. K. Pecharsky, K. A. Gschneidner, A. D. Caplin, and L. F. Cohen, "Identifying the critical point of the weakly first-order itinerant magnet DyCo$_2$ with complementary magnetization and calorimetric measurements," Phys. Rev. B **87**, 134421 (2013).

[16]V. Basso, C. P. Sasso, G. Bertotti, M. LoBue, L. Morellon, and C. Magen, "Predictions of AMR refrigeration cycles on Gd-Si-Ge alloys," in *Refrigeration Science and Technology Proceedings, IIR-IIF, N.2007-1*, edited by A. Poredos and A. Sarlah (2007), pp. 263-270, ISBN: 978-2-913149-56.

[17]K. P. Skokov, K.-H. Müller, J. D. Moore, J. Liu, A. Yu. Karpenkov, M. Krautz, and O. Gutfleisch, "Influence of thermal hysteresis and field cycling on the magnetocaloric effect in LaFe$_{11.6}$Si$_{1.4}$," J. Alloys Compd. **552**, 310 (2013).

[18]L. von Moos, C. R. H. Bahl, K. K. Nielsen, and K. Engelbrecht, "The influence of hysteresis on the determination of the magnetocaloric effect in Gd$_5$Si$_2$Ge$_2$," J. Phys. D: Appl. Phys. **48**, 025005 (2015).

[19]V. Basso, C. P. Sasso, K. P. Skokov, O. Gutfleisch, and V. V. Khovaylo, "Hysteresis and magnetocaloric effect at the magnetostructural phase transition of Ni-Mn-Ga and Ni-Mn-Co-Sn Heusler alloys," Phys. Rev. B **85**, 014430 (2012).

[20]K. G. Sandeman, "Magnetocaloric materials: The search for new systems," Scr. Mater. **67**, 566 (2012).

[21]M. E. Wood and W. H. Potter, "General analysis of magnetic refrigeration and its optimization using a new concept: Maximization of refrigerant capacity," Cryogenics **25**, 667 (1985).